JOURNAL OF SOLID STATE CHEMISTRY 49, 269–284 (1983)

Long Period Superstructures in Cu Intercalated VS_2: $Cu_{0.75}VS_2$[1]

D. COLAITIS,* D. VAN DYCK,† P. DELAVIGNETTE,‡ AND S. AMELINCKX*,‡

**E.R. 210, CNRS, 1 Place A. Briand, 92190 Meudon-Bellevue, France; †Rijksuniversitair Centrum Antwerpen, Groenenborgerlaan 171, B-2020, Antwerpen, Belgium; and ‡S.C.K./C.E.N., B-2400 Mol, Belgium*

Received November 29, 1982; and in revised form April 14, 1983

In $Cu_{0.75}VS_2$, a phase transition exhibiting a large temperature "hysteresis" is found below room temperature. Electron diffraction and microscopy show that, below the transition temperature, a one-dimensional superstructure is formed, the crystal being fragmented into domains belonging to three orientation variants. A model for the superstructure within one variant is proposed in which the Cu atoms are assumed to occupy strips of the two families of tetrahedral interstices within the same Van der Waals gap. Within the strips, the room temperature ordered structure is formed. Adjacent strips are separated by a type of APB planes which, if regularly spaced give rise to the superstructure. This model seems to be confirmed by computer generated diffraction patterns. Although it is generally believed that the presence of incommensurate reflections in these compounds is associated with the formation of a deformation modulated structure, this work shows that the long period antiphase boundary model (LPAPB) provides an alternative explanation. Physical arguments in favor of the LPAP model are also given, although some questions still remain to be answered.

1. Introduction

The structure and the physical properties of the compound $Cu_{0.75}VS_2$ have been studied by Le Nagard *et al.* (*1*). In this compound, the intercalated Cu atoms occupy ordered positions in the tetrahedral sites of the Van der Waals gap between two VS_2 layers. Certain physical properties such as the electrical resistivity show an anomalous behavior as a function of temperature which, according to these authors, could possibly be explained by the presence of a CDW, in analogy with other transition metal dichalcogenides. It is the goal of this work to use electron microscopy in order to follow the changes in this system as a function of temperature.

2. Structural Considerations

According to (*1*) the room temperature ordered phase of $Cu_{0.75}VS_2$ is monoclinic with space group $Bm - C_s^3$ and unit cell parameters $a_m = 1.1602$ nm, $b_m = 0.7325$ nm, $c_m = 0.6657$ nm, $\gamma = 121.83°$ with $Z = 8$; this phase will be hereafter called the m-phase.

The structure can be described as an fcc matrix of sulfur atoms in which the vanadium atoms occupy the octahedral sites between two close packed layers of sulfur,

[1] Work performed under the auspices of the association RUCA-SCK and with financial support of the I.I.K.W., also under the auspices of the international exchange relations between Belgium and France.

0022-4596/83 $3.00

similar to most of the layered transition metal dichalcogenides. However, it should be noted that the pure VS_2 structure which is of the $CdCl_2$ type (and not CdI_2 as mentioned in (*1*)) does not occur in nature without intercalation. The Cu atoms occupy 6 of the 8 tetrahedral interstices of the same type between two successive VS_2 sandwiches, whereas the tetrahedral sites of the other type remain empty. Figure 1 schematically shows the (001) projections of the monoclinic unit cell with the positions of the different atoms referred to the fcc matrix.

The stacking of (010) layers (roughly perpendicular to $[130]_m$) can be represented by the sequence

. . . b A β B a C α A c B γ C b . . .

in which A, B, C represent the sulfur atoms; a, b, c the vanadium atoms; and α, β, γ the copper atoms.

From Fig. 1 it is clear that the structure can also be described using a pseudo-orthorhombic unit cell with the same *a* and *c* parameters and with the *b* parameter equal to $[130]_m$. In this description the structure can easily be represented in a $[010]_0$ projection, which is shown in Fig. 2a for the Cu atoms only and in Fig. 2b for the V atoms only. The comparison between Figs. 2a and b allows one to represent the relative positions of Cu and V atoms of neighboring layers. As shown in (*1*) the V atoms, adjacent to tetrahedral vacancies, are not displaced in the $(010)_0$ plane, whereas the other V atoms slightly approach one another so as to form triangles, as shown by dashed lines in Fig. 2b.

3. Specimen Preparation

The material is prepared by heating the constituents in a sealed quartz tube accord-

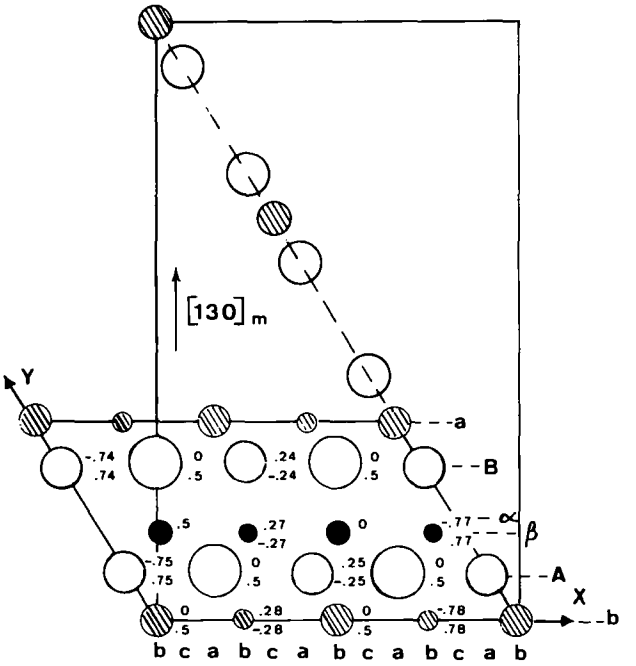

FIG. 1. (001) Projection of the primitive monoclinic unit cell, according to (*1*). The symbols are ◍, V; ○, S; ●, Cu. The stacking symbols with respect to the fcc matrix are also indicated. The structure can also be described as pseudo-orthorhombic with the *y* axis along $[130]_m$. Smaller circles are for $z = 0$ larger circles represent $z = \frac{1}{2}$.

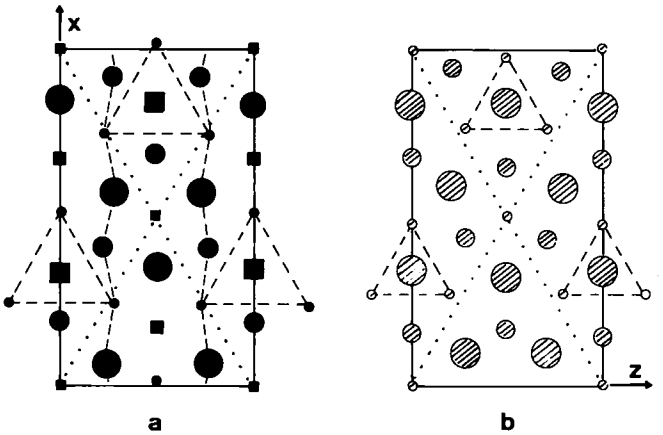

FIG. 2. $[010]_o$ projection of the pseudo-orthorhombic unit cell, according to (*1*). (a) Only the Cu atoms are indicated. The Cu atoms are slightly displaced so as to form zigzag lines instead of planes of constant z (slightly exaggerated on the drawing). (b) Only the V atoms are shown. The V atoms close to the tetrahedral vacancies are not displaced whereas the other V atoms are approaching one another so as to create triangles (shown by dashed lines).

ing to the reaction

$$3Cu_2S + 4V_2S_3 + S \rightarrow 8Cu_{0.75}VS_2.$$

The temperature is raised slowly to about 300–400°C in order to facilitate diffusion of sulfur and to avoid high vapor pressures. The tube was subsequently heated at a temperature of 850°C (somewhat below the melting temperature) for 15 days. A microcrystalline powder is formed, consisting of a mixture of the monoclinic phase $Cu_{0.75}VS_2$ and of the spinel phase $Cu_{0.5}VS_2$ (*2*) which can be identified by electron diffraction. The specimens are crushed, they do not present a preferential cleavage along the $(010)_o$ plane so that tilting is often necessary in order to obtain the $[010]_o$ zone.

4. Experimental Observation

4.1. General Characteristics of the Diffraction Pattern

The electron diffraction patterns of the phases $Cu_{0.75}VS_2$ and $Cu_{0.5}VS_2$ are very similar; they can only be distinguished on the basis of a small number of reflections that are present in the former but forbidden in the latter.

The [110] zone diffraction pattern of $Cu_{0.75}VS_2$ shows strong reflections related to the fcc matrix of sulfur but to which also copper and vanadium atoms contribute, and weak superstructure reflections caused by Cu and V atoms only (Fig. 3a). In general, the contribution of the Cu atoms to the electron structure factors F (*hkl*) of the fcc reflections (e.g. (004)), as well as the contribution of the V atoms to the electron structure factors of the superstructure reflections (e.g. (200)) is small as shown in Table I.

On cooling the specimen below room temperature, each reflection reveals two major satellites with irrational positions

TABLE I

F(*hkl*) IN 10^{-2} nm^{-1}

hkl	S + V + Cu	S + V	Cu
004	1.83	1.39	0.44
002	0.23	0.04	0.27

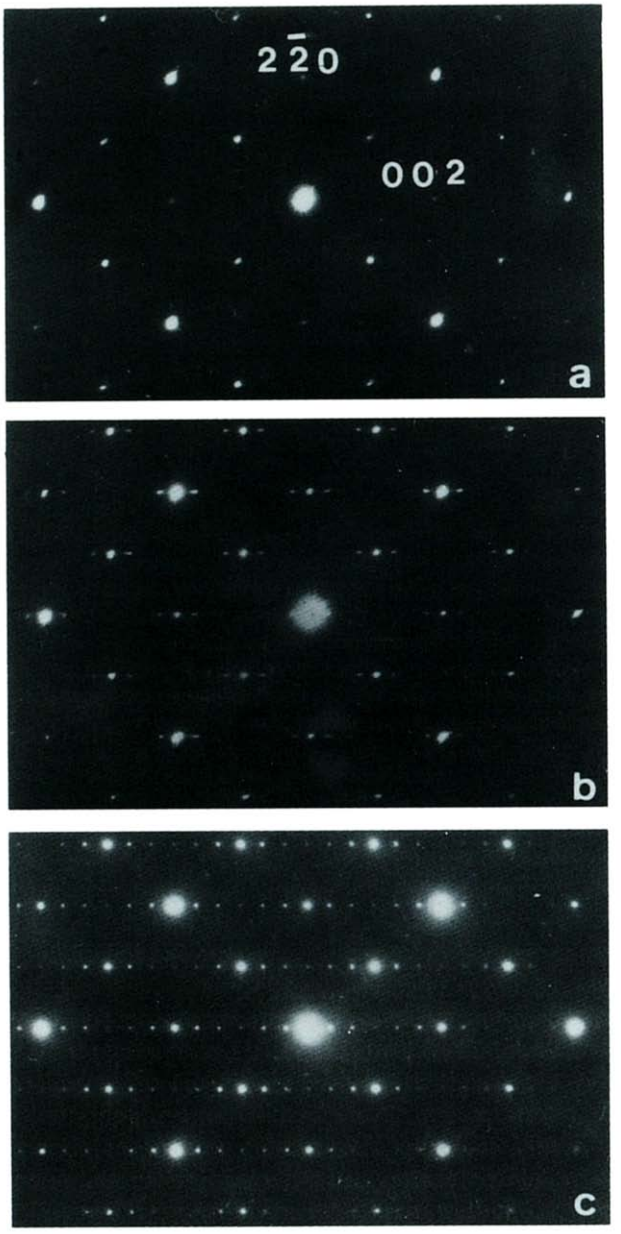

FIG. 3. [110]* zone diffraction pattern. (a) The ordered monoclinic room temperature phase. (b) On cooling two major satellites appear on both sides of the basic reflections, not necessarily at rational positions. (c) Lock-in of the satellites at a commensurate position, corresponding with the ordered t-phase. All the higher order satellites are present.

aligned along $[001]^*_m$ and whose spacing apparently needs not to be commensurate with the monoclinic unit cell, but can vary as a function of local composition and/or thermal history (Fig. 3b) [110] zone. A similar effect has already been discussed in other systems (*3–8*). On cooling to −190°C followed by heating to 150°C *in situ* in the

electron microscope, the satellite spacing varies continuously and reversibly with a large hysteresis. Sometimes, the satellites settle near to a commensurate position which corresponds to a more stable intermediate phase. When the phase becomes ordered, i.e., when the satellites lock in at the commensurate positions the higher order satellites suddenly appear as also noted in (*7*) (Fig. 3c) [110] zone. In some specimens, the satellites are already present at room temperature, before starting the thermal treatment.

Figure 4 shows the diffraction pattern of the $[130]^*_m$ zone, i.e., viewed perpendicular to the hexagonal VS_2 layers. At room temperature, only the fcc matrix reflections and the monoclinic reflections are present (Fig. 4a). At low temperature, the satellites appear (Fig. 4b). However, two kinds of satellite rows can be distinguished. In the $[001]^*_m$ row and in the even numbered rows parallel to $[001]^*_m$, the spacing of the most intense satellites seems to be doubled as compared to the satellite spacing of the odd rows. In the $[001]^*_m$ row, the faint odd satellites, can be completely extinguished by tilting the specimen, indicating that they are due to multiple diffraction.

4.2. Temperature Dependence of the Satellite Positions

Figure 5a shows a systematic $[001]^*_m$ row in which mainly two weak satellites appear on both sides of each basic reflection. On decreasing the temperature, the distance between the satellites and the basic reflections varies monotonically between 0 and a value somewhat over $\frac{1}{3}$ of the distance between two basic reflections. However, in the immediate vicinity of the basic reflections, the satellites can hardly be observed. At low temperature, the satellites lock in at $\frac{1}{3}$ giving rise to an ordered phase, called the t-phase. On increasing the temperature, the satellites again move toward the basic reflections. This process can be repeated reversibly with a large hysteresis, which makes it possible to maintain the t-phase up to room temperature.

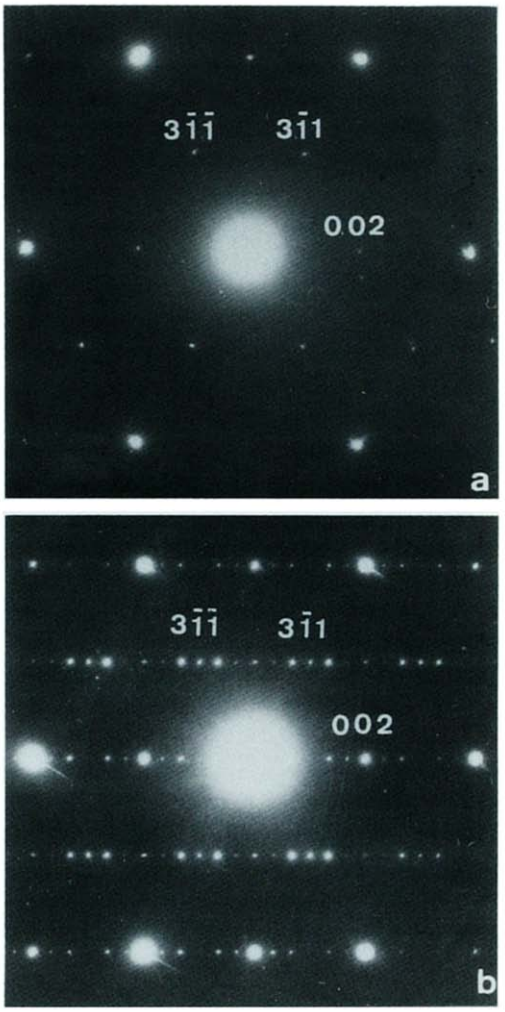

FIG. 4. Diffraction pattern of the $[130]^*_m$ zone, i.e., perpendicular to the hexagonal VS_2 layers. (a) At room temperature. (b) At low temperature revealing the satellites. The spacing of the major satellites is doubled in the even numbered rows (k = even).

Figure 5b shows an odd row parallel to $[001]^*_m$. Here the satellite spacing apparently is halved, and the satellites are relatively intense. On cooling, the satellites move from the basic reflections toward a value somewhat over $\frac{1}{6}$. When the t-phase is locked in at low temperature all the higher

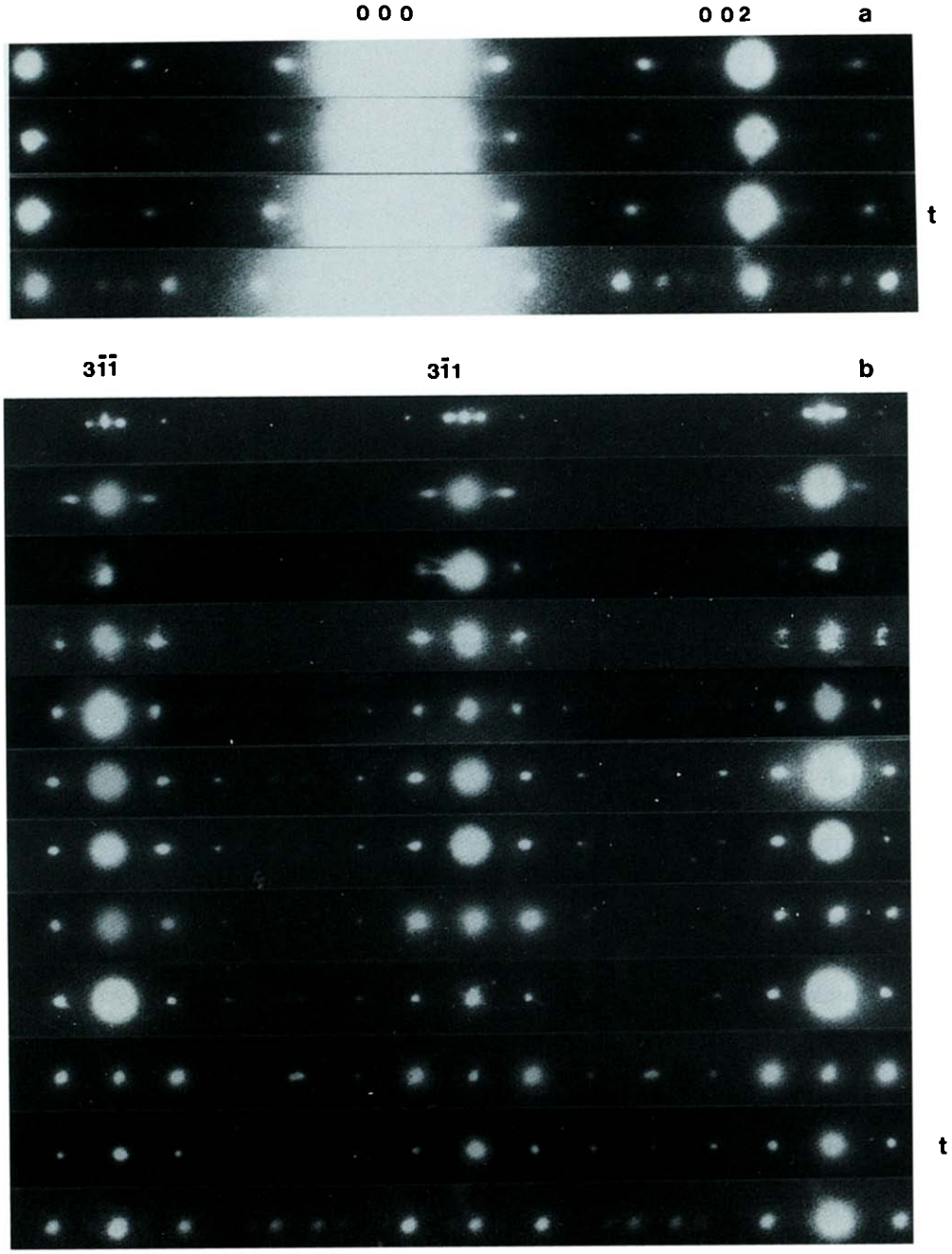

FIG. 5. (a) Systematic $[001]^{*}_{m}$ row without double diffraction spots, on decreasing temperature (from top to bottom) the satellites drift continuously. (b) First odd row parallel to $[001]_{m}$ with halved satellite spacing. Low temperature t-phase is indicated. The same behavior as a result of temperature variations as in (a) is presented.

order satellites appear, an effect which, as already mentioned, is a sensitive indication of the degree of order (*7*).

4.3. Domain Structures

In general, the satellite reflections are observed simultaneously along three equivalent rows, enclosing an angle of 120° with one another (Fig. 6a). Figure 6b shows a long exposure diffraction pattern taken at low temperature. In Figs. 6a and b, the satellite spacing is the same along the different rows. Figure 6c shows a diffraction pattern in which two families of satellites are in-

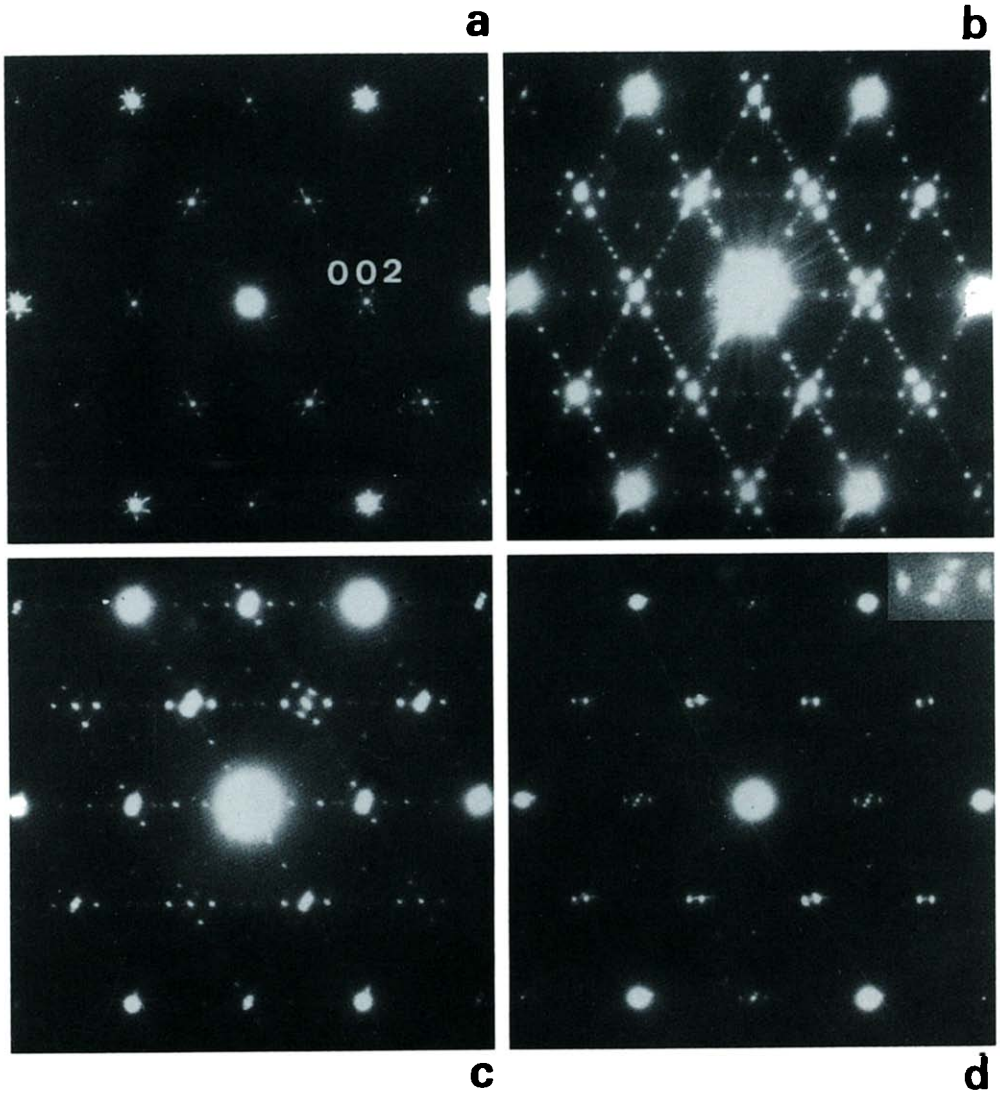

FIG. 6. Diffraction patterns of the $[130]_m$ zone at low temperature. (a) The satellites are present along three symmetrical directions. (b) Diffraction pattern (long exposure) at lower temperature. Higher order spots appear. The spacing is incommensurate. (c) One family of satellites has a different spacing and corresponds to a different degree of order. (d) The satellites have come closer to the basic spots at somewhat higher temperatures.

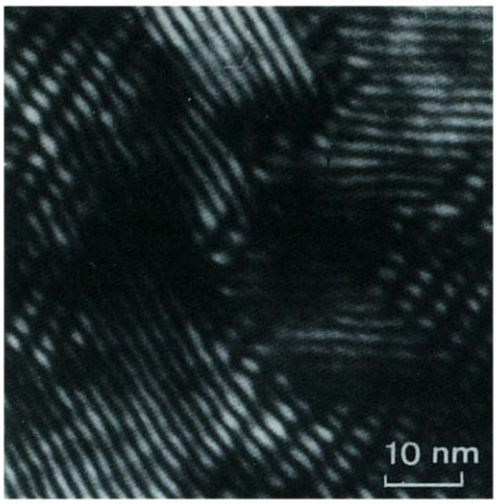

FIG. 7. DF electron micrograph showing two different types of domains with 1.8-nm fringes.

tense whereas the third is hardly observable, corresponding to a different state of order. Figure 6d shows a diffraction pattern in which only two families are present with different satellite spacings, as is clear from the inset. In all cases, the spacing in the even rows is doubled. These diffraction patterns suggest the existence of three orientation variants corresponding to the three families of satellites.

Figure 7 shows a dark field electron micrograph made with spots along the intersection of two odd rows; two families of 1.8-nm fringes can be distinguished separately, confirming the existence of domains in two directions.

Figure 8a shows the diffraction pattern of the $[140]^*_m$ zone which is only slightly inclined with respect to the $[130]^*_m$ of Fig. 6. Here the satellites can still be observed, giving rise to a pseudo-hexagonal star around the basic reflections, which, at first sight, seems peculiar in an otherwise rectangular diffraction pattern. Figure 8a is taken during the motion of the satellites; hence, the satellite spots are elongated. During the recording of Fig. 8b the satellite positions were stationary and the satellites are therefore sharp.

Figure 9 shows dark field images (selected beam shown in the inset) obtained from a single domain. Figure 9a is the lower temperature t-phase. Since only two satellites contribute to the image, fringes with a

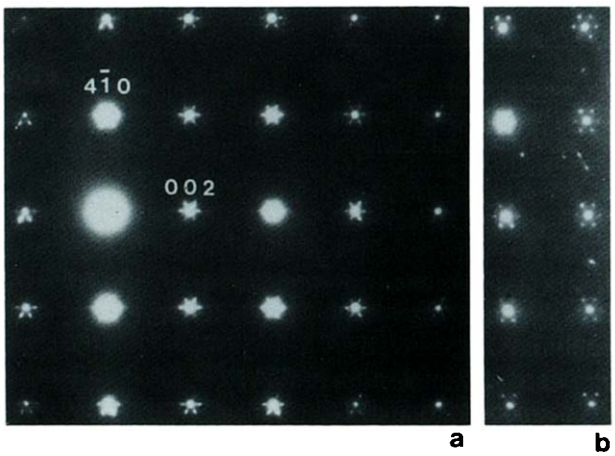

FIG. 8. Diffraction pattern of the $[140]_m$ zone, slightly inclined to the $[130]_m$ zone of Fig. 6. The satellites give rise to a pseudo-hexagonal star around the reflections of this rectangular diffraction pattern. (a) Dynamical recording: the motion of the satellites results in elongated spots. (b) Stationary diffraction pattern.

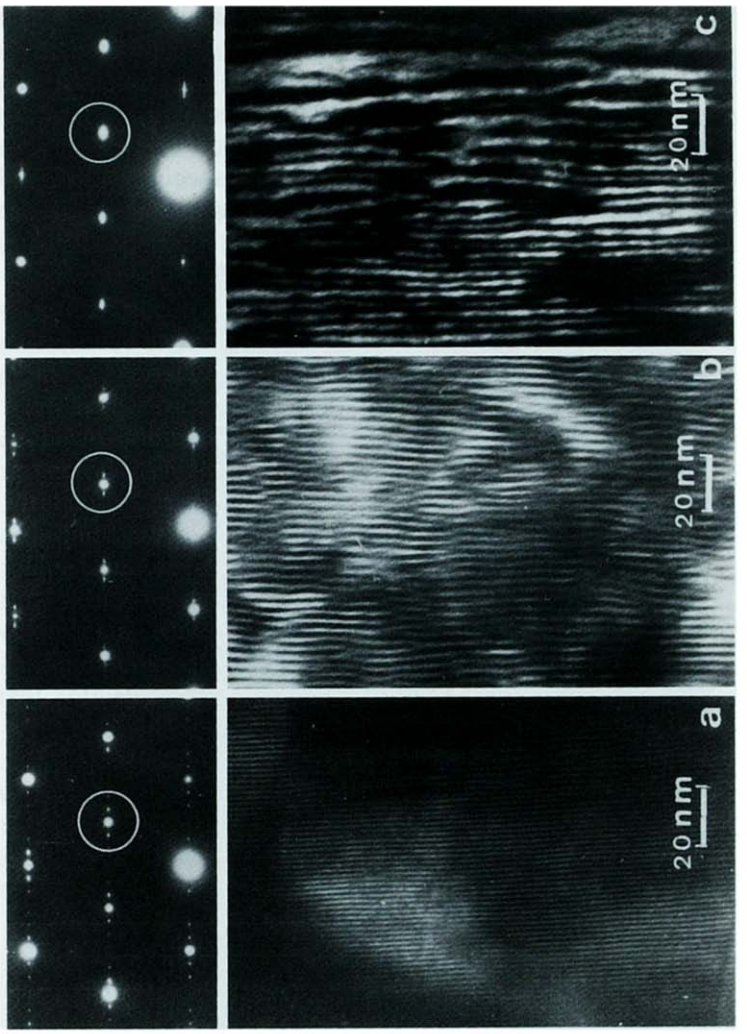

FIG. 9. High resolution electron micrographs (the imaging reflections are shown in the inset). (a) Low temperature ordered t-phase. (b) Higher temperature disordered phase. (c) Disordered phase at about room temperature.

sinusoidal intensity distribution are formed. On increasing the temperature, the fringe spacing increases and becomes more irregular (Fig. 9b). At room temperature the fringes become widely separated and irregular (Fig. 9c) and disappear completely at high temperature.

Figure 10 shows an intermediate state revealing fringes with mixed spacing.

4.4. Determination of Composition

The composition was determined using X-ray dispersive analysis (TRACOR). In general, the accuracy of an absolute composition determination is relatively poor (of the order of 10%) due to the fact that certain parameters are not accurately known. The composition was measured for two adjacent particles respectively of $Cu_{0.5}VS_2$ and $Cu_{0.75}VS_2$ which could be distinguished from their diffraction patterns. If the material parameters were adjusted so as to obtain the nominal composition of $Cu_{0.50}VS_2$ for the first particle one obtains a composition of $Cu_{0.75\pm0.05}VS_2$ for the second. From these values it can be concluded that, within the precision of the measurements, which seems to be satisfactory, the composition of the specimen $Cu_{0.75}VS_2$ showing the characteristic satellites, is the same as

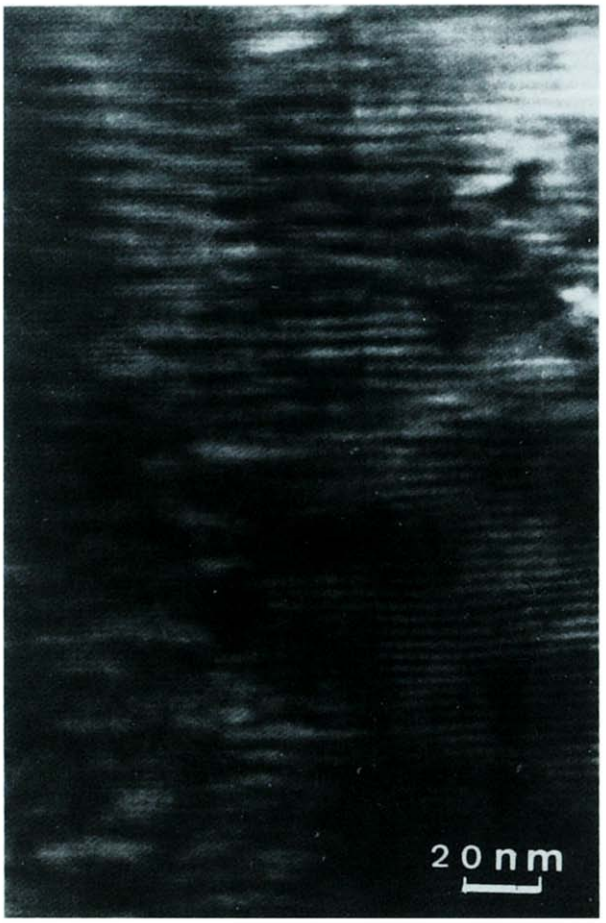

FIG. 10. High resolution electron micrograph showing a mixture of fringe spacings corresponding with a mixed phase.

the theoretical composition of the room temperature ordered phase, as reported in (*1*).

5. Model

5.1. Interpretation of Satellite Configurations

Since the ordering of the copper atoms and vacancies takes place in the gap between the closed packed sulfur layers, it seems appropriate to analyze the diffraction patterns taken with the zone axis perpendicular to these planes, i.e., along $[130]_m$. Figure 6b shows such a diffraction pattern for the t-phase.

For reasons of simplicity we shall consider different characteristic aspects in order to propose a structure model.

(a) The satellites with the largest intensity are located in the neighborhood of the original positions of the monoclinic structure. (Fig. 5). It is thus likely that the ordered superstructure should be described as a rearrangement of the original monoclinic structure.

(b) The satellites are located on rows parallel to $[001]_m^*$ which can be explained by assuming that antiphase boundaries of the type (001) periodically occur in the monoclinic structure.

(c) However, some difficulty arises if one tries to determine the spacing between adjacent APB from the inverse satellite spacing, since apparently the spacing in the odd numbered rows is doubled with respect to that in the even numbered rows. (The faint satellites in the even rows are probably caused by double diffraction.)

In a first stage, however, we shall restrict ourselves to the doubly spaced satellites which also are also the most intense ones in the odd numbered rows. In a second stage, the appearance of the extra satellites will be considered.

The diffraction pattern is now schematically represented in Fig. 11a. For reasons of simplicity we define a new hypothetical reciprocal unit cell (in projection) which is based on the unit vectors $\vec{e}_x^* = [002]_m^*$ and $e_y^* = [3\bar{1}1]_m^*$. The corresponding projected unit cell in real space is depicted in Fig. 11b. The satellites in the diffraction pattern can now be explained by the occurrence of APB planes perpendicular to $\vec{e}_x^*$ with a repeat vector $3\vec{e}_x^*$. The displacement vector of the APB planes can be determined from the shift of the satellites with respect to the positions of the Bragg reflections of the basic structure (*9*). Hence the projection $\vec{R}$ of the displacement vector expressed in the $(\vec{e}_x; \vec{e}_y)$ unit cell obeys the relations

$$\vec{R} \cdot (1,0) = (R_x, R_y) \cdot (1,0) = 0 \rightarrow R_x = 0$$

$$\vec{R} \cdot (0,1) = (R_x, R_y) \cdot (0,1) = \tfrac{1}{2} \rightarrow R_y = \tfrac{1}{2}$$

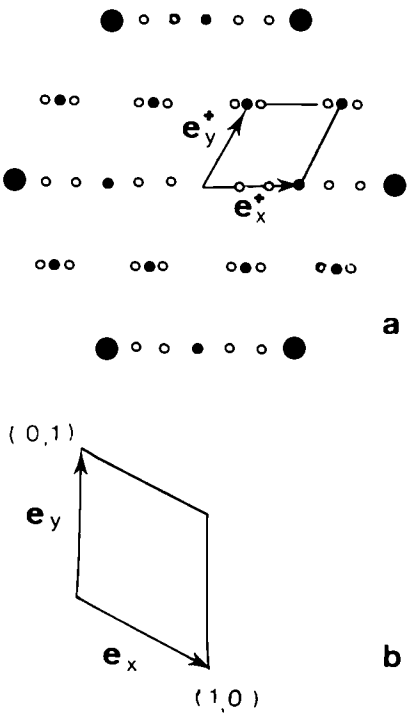

FIG. 11. (a) Schematic representation of the diffraction pattern of the $[130]_m$ zone. New reciprocal unit vectors are defined, which are more appropriate. (b) The corresponding unit cell in real space.

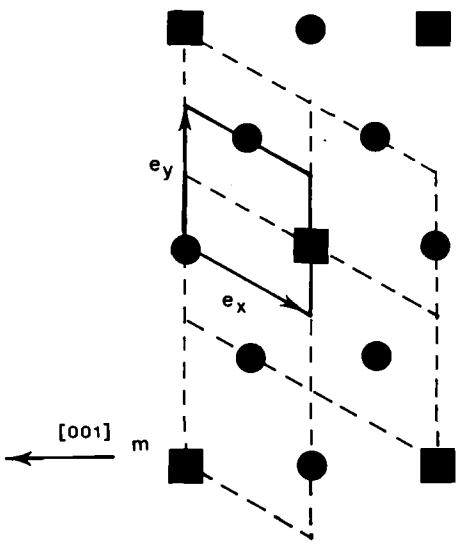

FIG. 12. Lattice spanned by the new unit vectors, onto which the tetrahedral site lattice is superimposed.

from which $\bar{R} = (0, \frac{1}{2})$ modulus a vector of the lattice $(\bar{e}_x, \bar{e}_y)$. If one assumes that the copper atoms are always situated in the tetrahedral sites between the S layers, the displacement vector needs to be a vector which connects two tetrahedral sites within the same layer. Figure 12 shows the lattice spanned by $\bar{e}_x$ and $\bar{e}_y$ onto which the tetrahedral site lattice is superimposed. It is clear that apart from equivalent vectors, the only displacement vector which satisfies the requirements is $\bar{R} = (0, \frac{3}{2})$ as indicated. This vector interconnects nearest tetrahedral sites and is parallel to the APB planes. The APBs can thus be conservative, in accordance with the reversible experiments of Section 4.1.

5.2. *Structure Model*

It is clear that the structure should contain antiphase boundary planes in the monoclinic structure perpendicular to the satellite rows, with a periodicity given by the inverse satellite spacing and the displacement vector deduced in the foregoing paragraph. This displacement vector $\bar{R} = (0, \frac{3}{2})$ need not necessarily be associated with one single APB but can be the resultant of a periodic series of successive APB for which the sum of the displacement vectors in one period equals $\bar{R}$.

Two cases can now be distinguished:

(i) The Cu atoms are all located in tetrahedral sites of the same type, i.e., in one close packed layer. In this case, the displacement vector which interconnects nearest tetrahedral sites cannot be decomposed. Hence, only one APB is present in the unit cell, as shown in Fig. 13. However, since the distance between neighboring vacant sites on both sides of the APB is different from that of the perfect structure, this model is not very probable.

(ii) The Cu atoms occupy both types of tetrahedral sites, i.e., the two close packed layers can be filled alternately with slabs of the monoclinic superstructure limited by APBs. The slabs are shifted one against the other over a vector $\bar{r}$ which interconnects two tetrahedral sites of different layers. Hence considering only the projection in the $(130)_m$ plane their total displacement vector $\bar{R} = (0, \frac{3}{2})$ is now decomposed into two partial displacement vectors $\bar{R} = \bar{r} + (\bar{R} - \bar{r})$. Four decompositions are now possible (apart from equivalent vectors):

(1) $\bar{r} = (-\frac{1}{2}, -\frac{1}{2})$	Fig. 14a
(2) $\bar{r} = (\frac{1}{2}, 0)$	Fig. 14b
(3) $\bar{r} = (0, -1)$	Fig. 14c
(4) $\bar{r} = (0, \frac{1}{2})$	

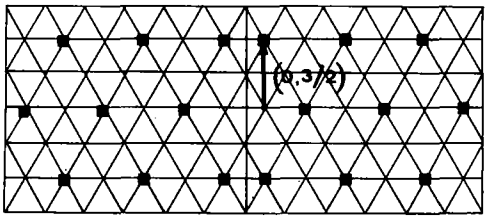

FIG. 13. Antiphase boundary with the derived displacement vector in a structure in which the Cu atoms occupy only one type of tetrahedral layer. Only the vacancies are indicated.

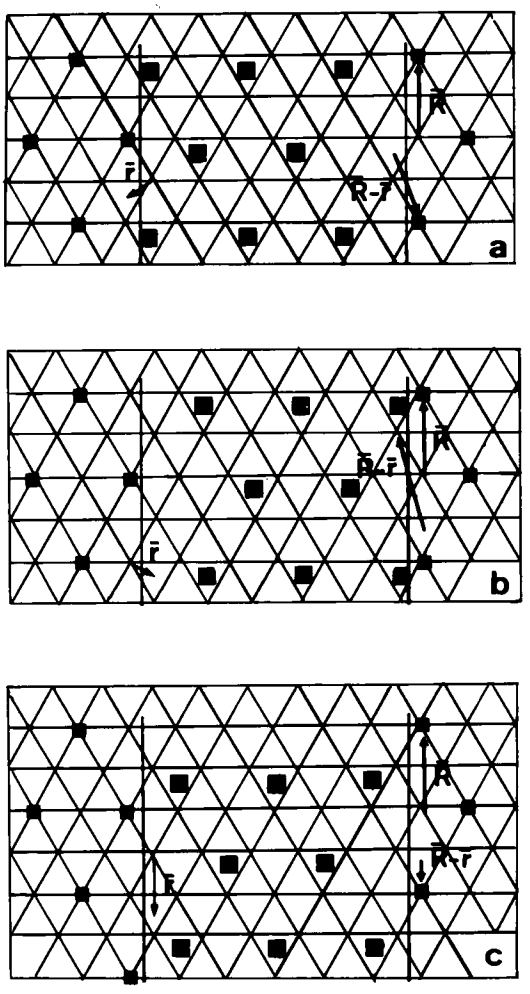

FIG. 14. Three possible models of pairs of APBs yielding the described displacement vector $\bar{R}$, in which the slabs of ordered m-phase alternately occupy one or the other type of vacancy layers. Only the vacancies are indicated.

In two cases, (1) and (2), the partial displacement vector $\bar{r}$ is not parallel to the APB. As a result, although the total composition remains unaltered, the individual APBs are nonconservative, and the distance between neighboring vacancies on both sides of the APB are rather different from those of the perfect monoclinic structure. Hence, these structures are not likely to occur. In cases (3) and (4), which are symmetrically related, the displacement vector $\bar{r}$ is parallel to the APB, so that the APB is conservative (in Fig. 14c only case (3) is shown). Furthermore, the nearest neighbor distance between vacant sites is approximately the same as that in the perfect structure, so that this model has our preference.

5.3. Refined Model for the t-Phase

The t-phase is particularly suitable for a refinement of the model as previously described, since its diffraction pattern contains a larger number of reflections of appreciable intensity. In the following, we shall compare the experimental diffraction pattern (Fig. 4b) with computer generated kinematical diffraction patterns in order to refine the model.

As in the preceding paragraph, the t-phase can be considered as being generated by pairs of APBs of the type shown in Fig. 14c periodically repeated in the monoclinic structure, the distance between adjacent APB's being equal to $\frac{3}{4}[001]_m$.

Figure 15a shows a structure model in which the slabs between APB's represent the idealized monoclinic structure (without atom displacements). The simulated diffraction pattern only shows the double satellite spacing in each row, in which the original monoclinic reflections are absent (Fig. 16a). This doubling is caused by the fact that the total displacement vector $\bar{R}$ is a lattice vector of the idealized monoclinic structure.

In order to obtain the original monoclinic reflections in the odd rows, as experimentally observed, it can be assumed that the slabs represent the real monoclinic structure, where the V atoms are slightly displaced so as to create triangles and where the Cu sites, instead of lying in planes of constant z, constitute puckered planes with an *ac* projection as shown in Fig. 2a. Now the total displacement vector $\bar{R}$ is not a lattice vector of the real monoclinic structure

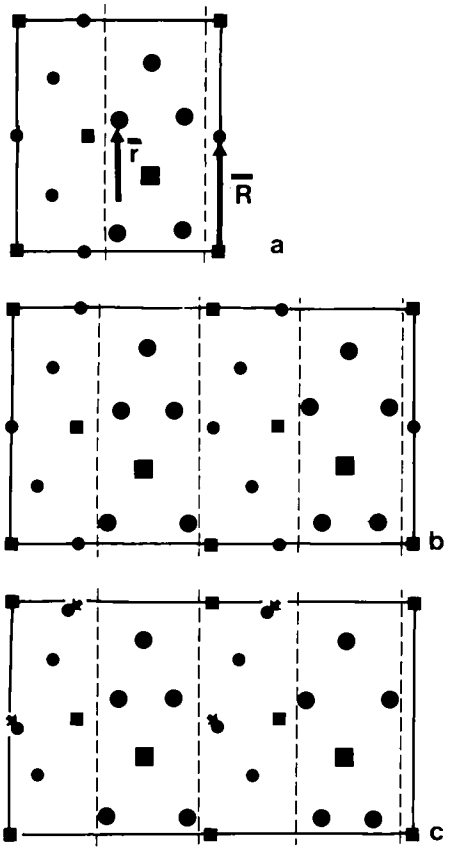

FIG. 15. Successive models used to refine the structure of the t-phase by comparing the computer simulated with experimental diffraction patterns. (a) Periodical APB in an idealized monoclinic structure. (b) Periodical APB in the real monoclinic structure. (c) With relaxation (arrows) at the APB planes.

(although 2 $\bar{R}$ still is), so that the original monoclinic reflections will appear and the satellite spacing in the odd rows will be halved. The displacement of the V atoms is of minor importance however, since they do not contribute strongly to these reflections. Figure 15b shows the structure model in which only the Cu atoms and vacant sites are shown (the displacements are somewhat exaggerated). Figure 16b shows the corresponding computer generated diffraction pattern which is already in good agreement with the experimental one.

There still remains some discrepancy to be solved. In the computer generated diffraction pattern of Fig. 16b no satellites are present along the systematic row through the origin since the projection of each slab

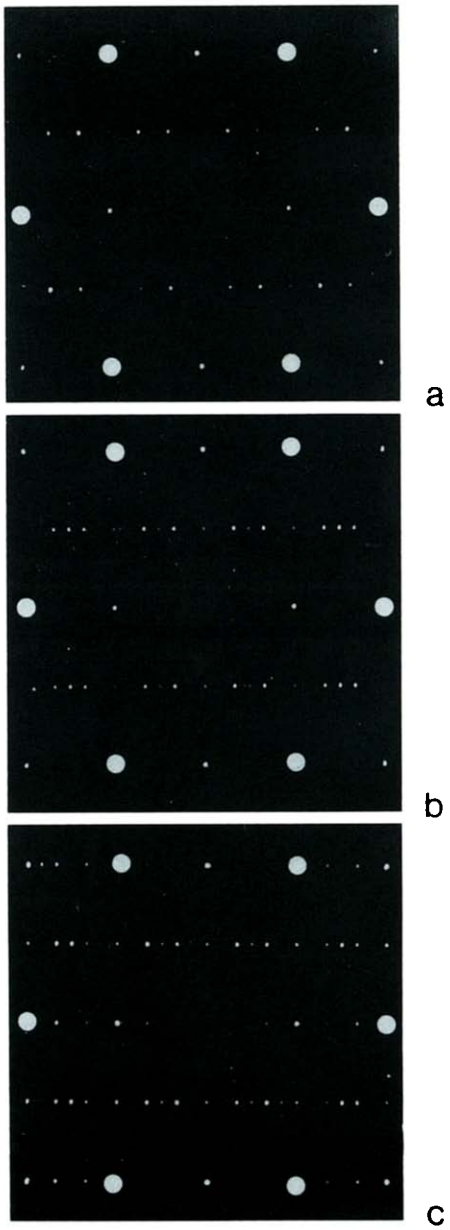

FIG. 16. Computer generated kinematical diffraction pattern. (a), (b), (c), respectively, correspond with the models of Figs. 15a, b, and c.

onto this axis is the same. In the experimental diffraction pattern however, these satellites are always present although very weak, even in the experimental situation where double diffraction is avoided. One can account for this effect by assuming relaxation effects along the APBs, e.g., so as to avoid too close Cu neighbors. Such an hypothetical model is given in Fig. 15c; with the direction and sense of relaxation denoted by arrows. The corresponding diffraction pattern is now in good qualitative agreement with the experiment (Fig. 16c).

5.4. Model for the Other Phases

The other $Cu_{0.75}VS_2$ phases, occurring at intermediate temperature, can be characterized by labeling the width of the lamellae between successive APB's in units of $\frac{1}{2}[001]_m$, hereby noticing that the number of units is always odd. In this respect the t-phase is denoted as $[3]^n$.

Figures 17a and b show the computer generated patterns of the phases $[5]^n$ and $[7]^n$, respectively, in which the higher order satellites in the odd rows are relatively weak. In fact, as can be shown from (*8*), the amplitude of the second-order satellite is only $\frac{1}{3}$ of that of the first-order satellite, and hence the intensity is relatively weak ($\sim\frac{1}{9}$). In the case of the phase $[3]^n$, the second-order satellites of two adjacent basic reflections coincide, giving an amplitude of $\frac{2}{3}$ and hence an intensity of $\frac{4}{9}$.

The presence of one major satellite in a pseudo-incommensurate position can be explained as corresponding with an intermediate state, consisting of an irregular mixing of slabs of different widths, the spacing of the satellite corresponding with the "average" width. The sharpness of the satellites is related to the variance of the distribution of slab widths; when the distribution is strongly peaked around the "average" width, the satellites remain relatively sharp (*5, 7, 10*). A lack of correlation in the distribution of these widths results in a drastic decrease of the intensity of the higher order satellites (*7*). At very low temperature, an almost perfectly ordered phase has been observed (Fig. 6b) which might be characterized as $[3^5\ 1]$.

A point to note is that when the major satellites approach the basic reflections, the average distance between APBs becomes very large. Hence, the satellites along the central row, which according to our model stem from relaxation effects at the APBs should become very faint. This effect has also been observed (see Section 4.2).

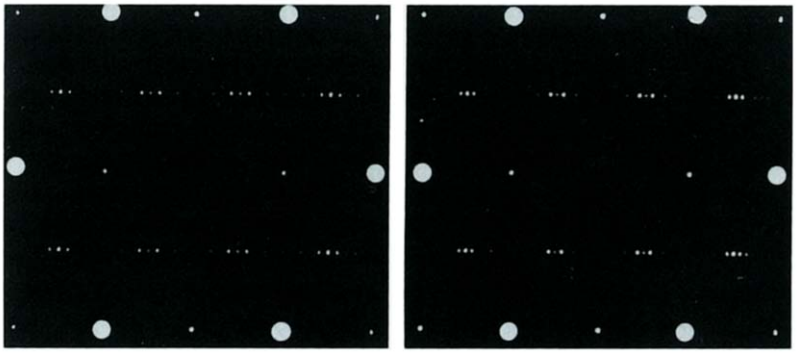

FIG. 17. Simulated diffraction patterns of the ordered phases $[5]^n$ and $[7]^n$. The second-order satellites, although sharp, are relatively weak.

6. Discussion

It has been shown thus far that the presence of incommensurate reflections shifting with temperature need not necessarily be explained by the formation of a one-dimensional deformation modulated structure but can also result from a long period antiphase boundary (LPAB) structure with an "average" APB distance. However, if one tries to make speculations that go beyond the purely descriptive stage, some problems remain unsolved and even seem to be contradictory.

Arguments in favor of the LPAPB model are that:

(i) It enables one to explain the occurrence of even very small q vectors (very large periods).

(ii) The mobility of the Cu atoms is still high enough below room temperature to explain the necessary Cu diffusion.

(iii) The assumed transformation requires atomic diffusion; this takes some time. For kinetic reasons some kind of temperature "hysteresis" is thus to be expected, i.e., the transformation will take place at a higher temperature during a heating cycle than during a cooling cycle.

However, at this stage, it seems difficult to explain the increasing concentration of APBs with decreasing temperature, an effect which might be influenced by various factors such as the energy associated with the formation of an APB, which is probably small; Fermi surface effects and entropy effects resulting from disorder in the APB distribution.

Acknowledgment

The authors thank Mr. A. Schallenberg for his valuable help by reproducing the figures and the photographs.

References

1. N. Le Nagard, G. Collin, and O. Gorochov, *Mater. Res. Bull.* **12,** 975 (1977).
2. N. Le Nagard, A. Katty, G. Collin, O. Gorochov, and A. Willig, *J. Sol. State Chem.* **27,** 267 (1979).
3. D. Colaïtis, P. Delavignette, D. Van Dyck, and S. Amelinckx, *Phys. Status Solidi A* **51,** 557 (1979).
4. D. Colaïtis, D. Van Dyck, P. Delavignette, and S. Amelinckx, *Phys. Status Solidi A* **53,** 423 (1979).
5. D. Van Dyck, D. Colaïtis, P. Delavignette, and S. Amelinckx, *Phys. Status Solidi A* **53,** 105 (1979).
6. D. Colaïtis, D. Van Dyck, P. Delavignette, and S. Amelinckx, *Phys. Status Solidi A* **58,** 271 (1980).
7. D. Van Dyck, C. Conde, and S. Amelinckx, *Phys. Status Solidi A* **56,** 377 (1979).
8. D. Van Dyck, C. Conde, and S. Amelinckx, *Phys. Status Solidi A* **58,** 451 (1980).
9. J. Van Landuyt, R. De Ridder, R. Gevers, and S. Amelinckx, *Mater. Res. Bull.* **5,** 353 (1970).
10. K. Fujiwara, *J. Phys. Soc. Jpn.* **12,** 7 (1957).